C11 In situ tailoring of carbon dots-metal ferrite nanohybrid as multipurpose marker agent of HeLa cancer cells

by Mochamad Zakki Fahmi

Submission date: 24-Mar-2023 03:02PM (UTC+0800)
Submission ID: 2045226514
File name: InSituTailoringOfCarbonDots-me_1.pdf (3.08M)
Word count: 6587
Character count: 35036

Journal of MATERIALS RESEARCH

Article
DOI:10.1557/s43578-022-00612-3

In situ tailoring of carbon dots-metal ferrite nanohybrid as multipurpose marker agent of HeLa cancer cells

Siti Febtria Asrini Sugito[1,2], Fakhri Firdaus[1,2], Yu Aung[1,2], Satya Candra Wibawa Sakti[1,2], Hsien-Tai Chiu[1,2], Mochamad Zakki Fahmi[1,2,a)]

[1] Department of Chemistry, Supramodification Nano-micro Engineering Research Group, Universitas Airlangga, Surabaya 60115, Indonesia
[2] Hsien-Tai Department of Chemistry, National Cheng Kung University, Tainan City 701, Taiwan
[a)] Address all correspondence to this author. e-mail: m.zakki.fahmi@fst.unair.ac.id

Received: 4 March 2022; accepted: 23 May 2022; published online: 2 June 2022

The development of multifunction material was considered to attain effectiveness on cancer treatment. The present study pursues the potential application of metal ferrite nanoparticles covered with CDs to get dual-active nanomaterial on fluorescent and magnetic responses that were prepared on a one-pot solvothermal method. Some analyses indicated the nanohybrids consisted of amorphous structure. Besides, the optical analysis performed optimum emission with QY percentage up to 0.9 and 0.6, respectively. Magnetic response assessment confirmed CDs@$MnFe_2O_4$-15 has good superparamagnetic properties with saturation magnetization value of 38.485 emu/g, while CDs@$CuFe_2O_4$-15 at 9.5245 emu/g. The DLS measurement showed an average size of CDs@$MnFe_2O_4$-45 at 63.98 nm, while CDs@$CuFe_2O_4$-45 at 55.46 nm. Then, this nanosized drive to perform good photoluminescent properties and good cytotoxicity due to the nanohybrids of CDs@MFe_2O_4-45 can easily enter the HeLa cells without harming its original structure. The above finding has well-proven good clinical potency of the nanohybrid as simultaneous fluorescent and magnetic-based detection.

Abbreviations

CDs	Carbon dots
MNPs	Magnetic nanoparticles
CDs-MNPs	Nanohybrid of carbon dots with magnetic nanoparticles
CDs@$MnFe_2O_4$	Nanohybrid of carbon dots with manganese ferrite oxide
CDs@$CuFe_2O_4$	Nanohybrid of carbon dots with copper ferrite oxide
Gd-TPA	Gadolinium-diethylenetriamine pentaacetic acid
MRI	Magnetic resonance imaging
QY	Quantum yield
Ms	Magnetization size

Introduction

The necessity on early detection was essential to reduce the prevalence of cancer. Clinically, diagnostic tests prefer to visualize stronger contrasts of tissues and organs imagined by MRI (Magnetic Resonance Imaging) [1, 2]. MRI technology as a non-invasive methodology has been an essential and valuable imaging technique in the field of biomedical applications that can minimize misdiagnosis of various medical conditions [3, 4]. Despite the excellent imaging of MRI, the role of the contrast agent is necessary, it has been the important element that needs to be marked to improve the sensitivity for the detection of injuries [5]. Commonly, Gd-DTPA (Gadolinium-Diethylene Triamine Pentaacetic Acid) is widely used as MRI contrast to enhance the signal of the aim tissues and body structures [6, 7].

MRI contrast agents have a core based on paramagnetic metal with a possibly outer coating from a biocompatible material and divided into T_1 and T_2 of enhancement mechanism. T_1 contrast agents are usually paramagnetic complexes with the process that can be accelerated to produce brighter T_1-weighted images [7, 8]. It is preferred for clinical diagnosis because the signal on MRI images is bright [9]. T_2 contrast agents are based on iron oxide nanoparticles, which are superparamagnetic [7]. The magnetic field accelerates the process of dephasing the nuclear spin of photons to disrupt the local magnet and produce a darker image [5, 9].

Gd-DTPA is a very great paramagnetic complex with high complex stability, low toxicity, and readily distributed to water

[10]. Despite the advantages of Gd-DTPA as an MRI contrast agent, Gd-DTPA has an unclear effect on the endocytosis process and Gd may exist in a free state with high toxicity when the complexing process is neglected [11, 12]. On the other hand, the cost of importing Gd-DTPA compound is relatively high that causes the diagnosis using MRI is valuable.

The metal ferrite nanoparticle MFe_2O_4 (M = Mn, Co, Ni, etc.) are magnetic compound nanoparticles that are primarily used for in-vivo and non-invasive applications to detect clinically important biological targets as highly sensitive [13–17]. One of the reasons for using magnetic nanoparticles as a marker required for contrast agents is the magnetism that can be used as a cellular target through external magnetic fields [18]. The particular physical and chemical characteristics of magnetic nanoparticles present them as fitting materials for biomedical research. Pharmaceutical chemistry and biomedical research have shown that magnetic nanoparticles exhibit magnetic properties at room temperature and are very useful [19].

Metal ferrite nanoparticle MFe_2O_4 synthesized via hydrolysis or non-hydrolysis approach showed superior magnetism and were used as an ultrasensitive as T_1 MRI contrast agent [20–22]. Nanoparticles play an important role in the magnetization of MRI contrast agents, but the image fluoresces insufficiently than the fluorescence of CDs. As demonstrated by MRI studies, coating magnetic nanoparticles with CDs revealed higher fluorescence images compared to magnetic nanoparticles [18, 23]. The CDs are attracting attention in the field of fluorescent sensors because of their great water solubility, excellent photostability, low toxicity, and superior biocompatibility [24–26]. This has led many researchers to use CDs as marker agents, biosensing, bioimaging, and drug delivery in medical field [27, 28].

Despite the numerous studies on CDs synthesis and its application in the imaging fields, research on CDs from ethanolamine is still lacking. In addition, some researchers have succeeded in synthesizing CDs from ethanolamine, showing good fluorescence results. Ethanolamine is suitable as a carbon source on N-doped CDs due to its abundant amino and hydroxyl groups [29]. Herein, high yields of CDs ethanolamine were successfully synthesized using a pyrolysis approach [29–31]. Further development of the previous synthesis led to the adoption hydrothermal approach that exhibits good dispersion stability in water and blue fluorescence emission [29].

The synthesis of CDs can be easily divided into a top-down and a bottom-up approach [24]. The bottom-up approaches link the fluorescence properties, by carefully designing molecular precursor structure and manufacturing process, it is an inducement to customize the CDs with well-defined size, variable surface state, and internal structure [29, 32]. On the other hand, top-down approaches are usually difficult to control the particle size, surface, and internal structure [29, 33]. The bottom-up methods of synthesis CDs can be further divided into hydrothermal, ultrasonication, microwaves, pyrolysis, and chemical thermal [34].

Furthermore, as precursors of CDs in metal ferrite nanoparticles are used for detection, the potential fluorescence of ethanolamine has been reported [31]. The properties of CDs ethanolamine provide high stability, abundant yields, and good solubility upon the water [35]. Despite the various advantages, the application of CDs ethanolamine has minimal reported use in the medical field. Researches on CDs synthesis are crucial for expanding the application of CDs in the sensing and imaging field [29]. It has been attempted to use magnetic nanoparticles and CDs as marker agents to defeat the problems of expensive precursors and emission loss, which are major factors in MRI contrast agents. No one has proposed the in-situ solvothermal approach of the nanohybrid using the two kinds of combination, mostly multisets, composites, and derivatives of the original properties of each nanoparticle.

In this study, we improve the synthesis of nanohybrid from metal ferrite nanoparticle and CDs ethanolamine and compare the metal Cu and Mn potential application as contrast agents in MRI. Of the various metal ferrite, the metals Mn and Cu ferrites are less toxic than other ferritic metals, so their potential is valuable and secure in medical applications [18]. The solvothermal approach is chosen because the yields are petite and distributed consistently. Therefore, the application of nanohybrid to cancer has become a pressing priority to observe cancer as a global disease that is still attracting global attention [36]. As a result, studies in toxicity and in-vitro assays of HeLa tumor cells were conducted to confirm that the nanohybrid could potentially be used as a simultaneous marker.

Result and discussion

Characterization of nanohybrids

The synthesis of the nanohybrid combines individual processes MFe_2O_4 and CDs. In particular, the synthesis of CDs initiated the rearrangement of ethanolamine at high temperatures. This treatment allows the molecule to form CDs with a graphene oxide-like structure in dehydration and carbonization, as shown in Scheme 1. This mechanism has the advantage that the process of reaching the high quality of CDs is simple.

During CDs@MFe_2O_4 synthesis, Mn and Cu elements were selected as the significant components in producing metal ferrite. The interaction of $Mn(acac)_2$–$Fe(acac)_3$ produced $MnFe_2O_4$, and interaction of $Cu(acac)_2$–$Fe(acac)_3$ produced $CuFe_2O_4$ by the solvothermal process. In contrast, oleylamine was used as a ligand for magnetic nanoparticles to stabilize and produce hydrophobicity [37]. This study performed CDs

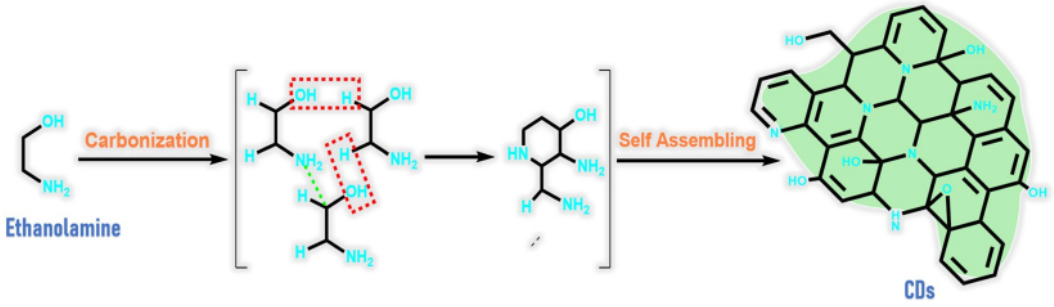

Scheme 1: Schematic illustration of ethanolamine self-assembling to form CDs.

synthesis using high temperatures called the solvothermal process shown in Scheme 2. After adding ethanolamine at 150 °C under the assumption that the reaction of Scheme 1. occurs, MFe_2O_4 covered with CDs is formed in this process as CDs@MFe_2O_4 nanohybrid. Therefore, nanohybrids can exhibit the optical properties of CDs and can have the ability to be magnetically induced due to the presence of magnetic nanoparticles with superparamagnetic properties [38].

CDs@MFe_2O_4 characterization is an essential part of demonstrating the successful nanohybrid synthesis process. Spectroscopy analysis was first to run to access the optical properties of the nanohybrid. Indeed, CDs@MFe_2O_4 served to elucidate the optical properties of nanohybrid. To prove the assumption, this study utilized UV–Vis absorption by varying the concentration of ethanolamine, as shown in Fig. 1. The spectrum showed that the maximum wavelengths of CDs@$MnFe_2O_4$ were 221 nm and 261 nm, CDs@$MnFe_2O_4$-15 was 259.6 nm, CDs@$MnFe_2O_4$-30 was 246.4 nm, and CDs@$MnFe_2O_4$-45 was 259.4 nm. However, the maximum wavelength of CDs@$CuFe_2O_4$-15 was 268 nm, CDs@$CuFe_2O_4$-30 was 270 nm, and CDs@$CuFe_2O_4$-45 was 272 nm. CDs absorbance peak showed an electron transition $\pi \rightarrow \pi^*$ as a core and an electron transition $n \rightarrow \pi^*$ as a surface state. CDs@$MnFe_2O_4$-30 and CDs@$CuFe_2O_4$-45 spectrum showed the highest absorbance with λ_{max} of 246.4 nm and 272 nm. This maximum wavelength implies an electron transition $\pi \rightarrow \pi^*$ C=C aromatic groups within the nucleus of CDs [39].

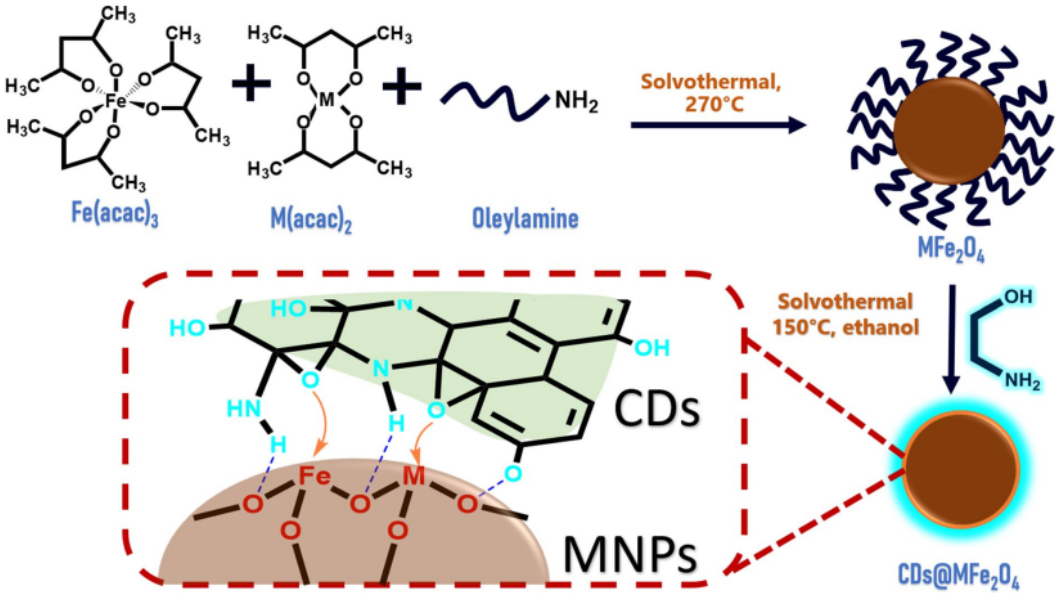

Scheme 2: Schematic illustration on synthesis mechanism of CDs@MFe_2O_4.

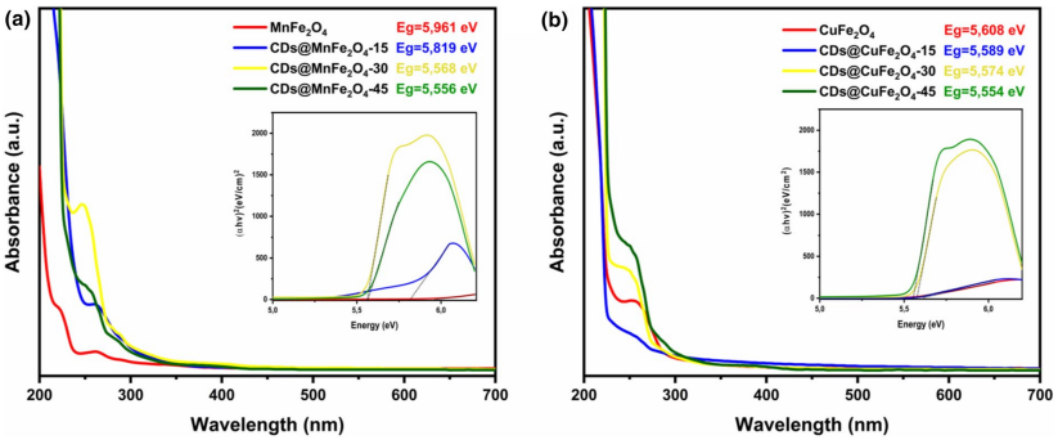

Figure 1: UV–Vis spectra of (a) CDs@$MnFe_2O_4$ and (b) CDs@$CuFe_2O_4$. Inset: the TAUC plot of each spectrum.

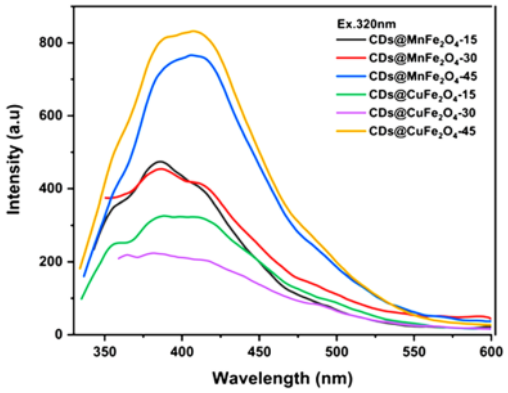

Figure 2: PL spectra of CDs@$MnFe_2O_4$-15, CDs@$CuFe_2O_4$-15 CDs@$MnFe_2O_4$-30, CDs@$CuFe_2O_4$-30, CDs@$MnFe_2O_4$-45, and CDs@$CuFe_2O_4$-45.

Further, in emission observation, the effects of various ethanolamine on nanohybrids can be accessed by photoluminescent instruments. Figure 2 showed the emission characteristics of nanohybrid CDs at excitation wavelengths of 320 nm. One of the characteristics of CDs is emission variation at specific wavelengths called excitation-dependent emission. Traps are known as defective due to an oxygenated group of CDs [40]. The existence of excitation-dependent emission occurs because the electron orbitals of the CDs are various, and emission will change regardless of the energy absorbed by the CDs. Different emission variations are caused by several factors, such as the structure of the CDs formation. In addition, increasing the concentration of ethanolamine in the nanohybrids will increase the emission of the formed nanohybrid. In particular, samples of CDs@$MnFe_2O_4$, CDs@$MnFe_2O_4$-15, CDs@$MnFe_2O_4$-30, and CDs@$MnFe_2O_4$-45 were analyzed at excitation wavelengths of 320, 340, 360, 380, 400, and 420 nm, which has the highest intensity at the emission wavelength (λ_{em}) of 320 nm. CDs@$MnFe_2O_4$-15 and CDs@$MnFe_2O_4$-30 spectra could fluoresce at a wavelength of 386 nm, and CDs@$MnFe_2O_4$-45 fluoresce higher at 406 nm, while CDs@$CuFe_2O_4$-45 had the highest intensity at the emission wavelength (λ_{em}) of 410 nm. The relative quantum yields (QY) of $MnFe_2O_4$ in CDs@$MnFe_2O_4$-15, CDs@$MnFe_2O_4$-30, and CDs@$MnFe_2O_4$-45 were 0.462%, 0.118%, and 0.9%, respectively. CDs@$CuFe_2O_4$-15, CDs@$CuFe_2O_4$-30, and CDs@$CuFe_2O_4$-45 showed that the QY of $CuFe_2O_4$ was 0.60%, 0.27%, and 0.005%. This indicates that the best fluorescent ability is CDs@$MnFe_2O_4$-45 and CDs@$CuFe_2O_4$-45 containing 45 mL ethanolamine. According to the study results, the addition of ethanolamine leads to an increase in the aggregation of ethanolamine during the formation of CDs. Therefore, graphene oxide is more likely to be formed. Copper increases the interaction between CDs and ethanolamine in $CuFe_2O_4$, which can destroy the original structure of copper itself. It happened because Copper has a higher binding affinity against the organic matter. Thus, aggregations may become high, which it can interfere with the absorbance tracing of CDs by UV–Vis spectroscopy and affect the QY values. To improve above results in which to evaluate contribution of CDs on featuring the optical properties, the observation potential band gap of the nanohybrids Fig. 1. Addition of ethanolamine result in increasing CDs area on nanohybrid that drive to decreasing band gap energy of bare metal ferrite (above 5.6 eV in average) to light area (below than 3.1 eV). CDs overs addition electronic orbital level in the metal ferrite smoothing photoluminescence process.

The FTIR analysis was performed to ensure the nanohybrids design structure of $MnFe_2O_4$-based and $CuFe_2O_4$-based nanoparticles shown in Fig. 3. The data specifically showed

the $MnFe_2O_4$ band at 586.6 cm^{-1} and 410.40 cm^{-1}, while the specific band at 644.22 cm^{-1} in both nanohybrid referred to the metal–oxide absorption [41]. In addition, oleylamine compounds were displayed in several wavenumbers, such as 2928.29 cm^{-1} for CH vibration and 1441.64 cm^{-1} for CN vibration [42]. Both nanohybrids revealed the existence of ethanolamine CDs at each specific band OH at over 3000 cm^{-1} and NH at 1579 cm^{-1} [43]. Therefore, these FTIR data clearly showed that all nanohybrids were composed of a combination of $MnFe_2O_4$, $CuFe_2O_4$ oleylamine, and ethanolamine nanoparticles.

The nanohybrid size distribution was further using Dynamic Light Scattering (DLS). The diagram and the graph in Fig. 4 show the average size and zeta potential. The average size of DLS was determined using the Polydispersity Index (PDI) parameter. The results indicated that the average size of $MnFe_2O_4$, CDs@$MnFe_2O_4$-15, CDs@$MnFe_2O_4$-30, and CDs@$MnFe_2O_4$-45 nanoparticles were 463.1 nm, 195.7 nm, 99.55 nm, and 63.98 nm, while the average size of $CuFe_2O_4$, CDs@$CuFe_2O_4$-15, CDs@$CuFe_2O_4$-30, and CDs@$CuFe_2O_4$-45 were 37.84 nm, 45.06 nm, 46.41 nm, and 55.46 nm. Excessive carbonation caused the nanoparticles to be aggregated, thereby forming large particles such as graphene oxide. Therefore, the role of temperature and time in the synthesis process was crucial for particle size control. The zeta potential values of $MnFe_2O_4$, CDs@$MnFe_2O_4$-15, CDs@$MnFe_2O_4$-30, and CDs@$MnFe_2O_4$-45 were − 0.3635 mV, 0.163 mV, 3.57 mV, and − 0.499 mV, while the values of $CuFe_2O_4$, CDs@$CuFe_2O_4$-15,

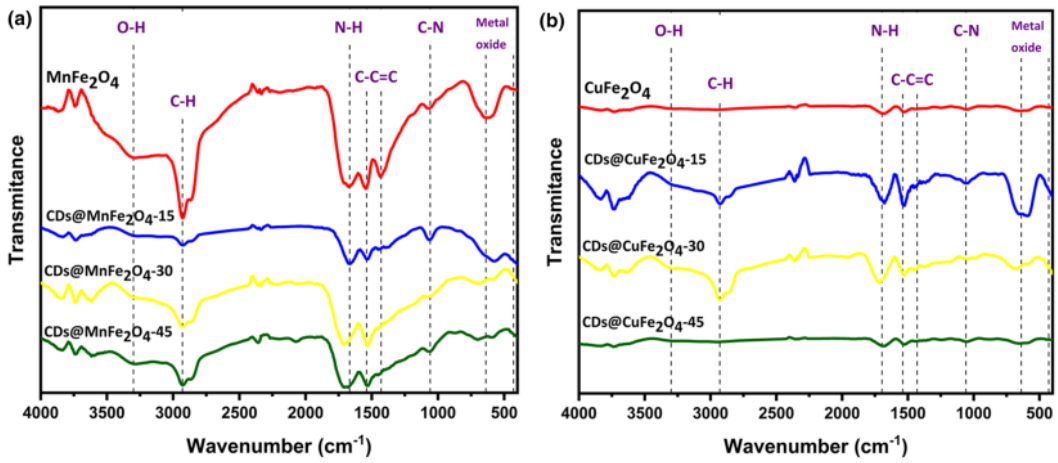

Figure 3: FTIR spectra of (a) CDs@$MnFe_2O_4$, CDs@$MnFe_2O_4$-15, CDs@$MnFe_2O_4$-30, and CDs@$MnFe_2O_4$-45; (b) CDs@$CuFe_2O_4$, CDs@$CuFe_2O_4$-15, CDs@$CuFe_2O_4$-30, and CDs@$CuFe_2O_4$-45.

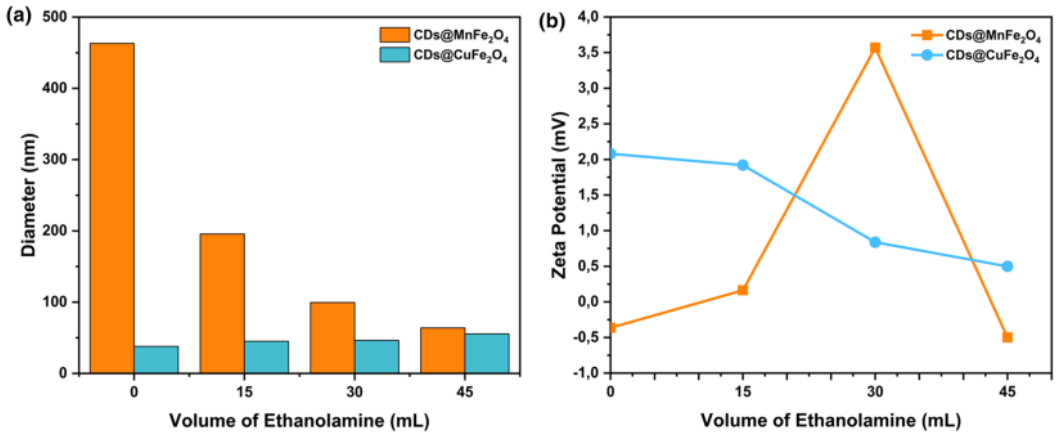

Figure 4: (a) DLS diagram of CDs@$MnFe_2O_4$-15 and CDs@$CuFe_2O_4$-15 and (b) Zeta potential graph of CDs@$MnFe_2O_4$-15 and CDs@$CuFe_2O_4$-15.

CDs@$CuFe_2O_4$-30, and CDs@$CuFe_2O_4$-45 were 2.08 mV, 1.92 mV, 0.838 mV, and 0.498 mV. Ethanolamine contains NH_2, increasing the potential zeta's value of nanoparticles [44]. $MnFe_2O_4$ and CDs@$MnFe_2O_4$-45 gave negative values due to the adsorption of OH ions or fats such as fatty amines and carboxyl groups on the surface of nanoparticles [37, 45]. Based on the DLS data, the smaller size of nanoparticle implied the bigger effectiveness as contrast agent application. The selected nanohybrids CDs@MFe_2O_4-45 were considered having the best properties as simultaneous marker and needed further analyses in toxicity assessment for clinical properties.

XRD analysis was used to determine the crystal structures and purity of the materials in solid. When the crystalline size was small, the diffraction peaks became wider because the small crystalline had a large X-ray reflection field [46]. Based on JCPDS 74-2403, $MnFe_2O_4$ had several 2θ peaks located at 29.6°, 34.9°, 42.4°, 52.6°, 56.1°, and 61.5°, while the JCPDS 010-0173 of $CuFe_2O_4$ had several 2θ peaks at 30.32°, 35.76°, and 57.36°. The enlarged the broad peak indicated the presence of CDs at 2θ of 19.20° as an amorphous structure of nanoparticles carbon leads caused by the loss of water molecules and material decomposition during the synthesis process [47].

CDs@$MnFe_2O_4$-15 had peaks at 35.13°, 42.78°, 56.14°, and 62.19°. CDs@$MnFe_2O_4$-30 had a broad peak of 2θ at 17.75°, which CDs@$MnFe_2O_4$-15 and CDs@$MnFe_2O_4$-45 did not have. The broadest peaks were owned by CDs, while the other peaks were 29.61°, 34.10°, 42.44°, 56.24°, and 61.79°. The diffractogram of CDs@$MnFe_2O_4$-45 had two peaks at 29.46° and 35.02°. These diffractograms are shown in Fig. 5.

The VSM was used to analyze the magnetic properties of a solid sample using a magnetic field in the range of −8 to +8 kOe. The graph of CDs@$MnFe_2O_4$-15 had a saturated magnetization value (M_s) at 38,485 emu/g with a coercivity value at 1.0975 G, and the M_s of CDs@$CuFe_2O_4$-15 was 95,245 emu/g with a coercivity value at 92,768 G that is shown in Fig. 6. The superparamagnetic shape had a specific magnetization value of 92 emu/g [48]. It concluded that CDs@MFe_2O_4-15 was classified as coated superparamagnetic because the magnetization is lower than the uncoated particles. This lowering is due to the smaller size of the coated particles and the ethanolamine as CDs was present on the surface of the particles.

Cytotoxicity assessment

The cytotoxicity test was used to determine the toxicity of a liquid sample by HeLa cells in-vitro. The principle of the MTT

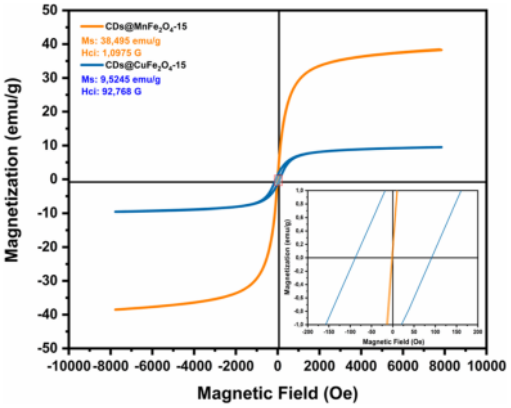

Figure 6: VSM spectra of CDs@$MnFe_2O_4$-15 and CDs@$CuFe_2O_4$-15. Inset: high magnification on adjusted area.

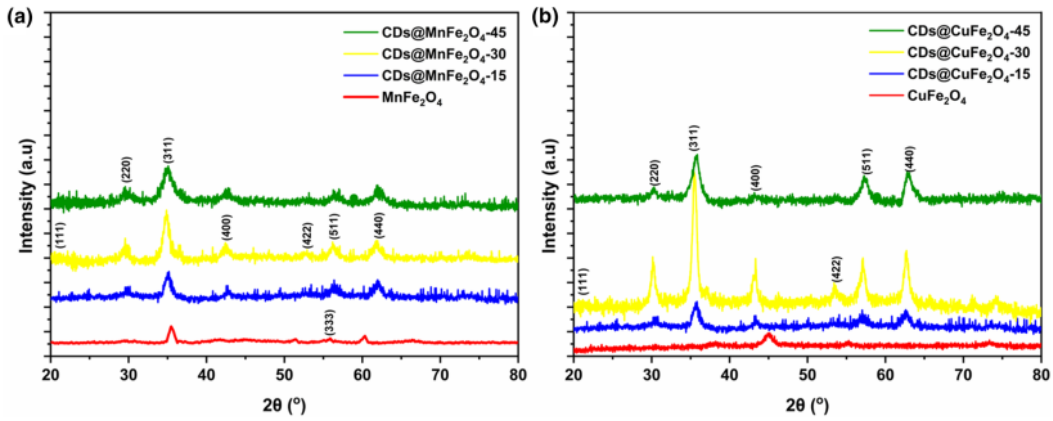

Figure 5: XRD diffractogram of (a) CDs@$MnFe_2O_4$, CDs@$MnFe_2O_4$-15, CDs@$MnFe_2O_4$-30, and CDs@$MnFe_2O_4$-45; (b) CDs@$CuFe_2O_4$, CDs@$CuFe_2O_4$-15, CDs@$CuFe_2O_4$-30, and CDs@$CuFe_2O_4$-45.

Assay method was reducing MTT salt (3-(4,5-dimethylthiazol-2-yl)-2,5-diphenyltetrazolium bromide) by dehydrogenation succinate enzyme in the mitochondria to form formazan. If the purple concentration produced was high, the toxicity level was low [49]. Materials with 80% or more cell viability at high concentrations were classified as non-toxic materials [43].

$CDs@MnFe_2O_4$-45 and $CDs@CuFe_2O_4$-45 had a high percentage of viability that was almost 90%, despite concentrations of up to 250 µg/mL caused by the preparation process. The preparation was carried out based on statistics, so the number of cells in the well was not precise. The percentage of cell viability at concentrations of 7.5, 15.5, and 31.5 µg/mL exceeded the control, and is shown in Fig. 7. $CDs@MnFe_2O_4$-45 and $CDs@CuFe_2O_4$-45 did not cause the decreased viabilit and drive evidence that the CDs on $MnFe_2O_4$ and $CuFe_2O_4$ nanoparticles will not harm cells [50].

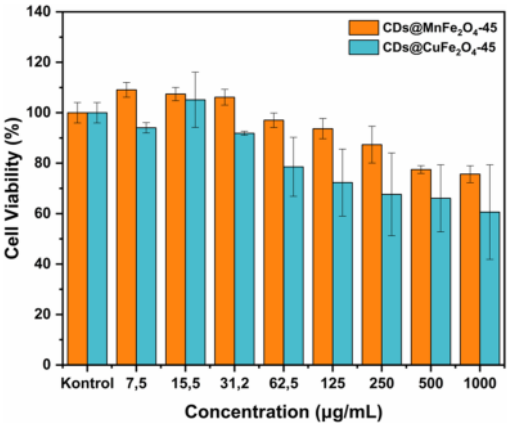

Figure 7: The viability percentage of HeLa cell on varying concentrations (7.50–1000 µg/mL) of $CDs@MnFe_2O_4$-45 and $CDs@CuFe_2O_4$-45.

Confocal laser scanning microscopy (CLSM)

CLSM is a method to analyze the internalization of CDs in HeLa cells, expressed by fluorescence intensity. In order to determine the location of the cell nucleus, it was necessary to add 4′6-diamino-2-phenylindol (DAPI) as a marker to produce a blue color [51].

Based on the results of the CLSM analysis, Fig. 8 shows that the NH_2 and –OH groups on CDs produced intracellular uptake through endocytosis of the folate receptors, because they were similar to the folate receptors. The internalization of CDs into the cytoplasm showed green fluorescence, indicating that CDs have entered the cell through endocytosis [50]. In addition, the role of DAPI in PBS (Phosphate Buffer Saline) was a control for determining the number and location of viable cells by staining, thereby showing blue fluorescence [52]. CLSM test results proved that $CDs@MnFe_2O_4$ and $CDs@CuFe_2O_4$ had good fluorescence and can be applied as candidates for simultaneous marker. Figure 8 shows the internalization of CDs into the HeLa cytoplasm of cells.

MRI imaging

MRI analysis was performed to assess the ability of the sample $CDs@MnFe_2O_4$ and $CDs@CuFe_2O_4$ to serve as a contrast agent. An active ingredient contrast will help in the longitudinal relaxation of water molecules by giving a positive signal effect, increasing the intensity of the T1-weighted image [37]. In this research, the analysis was assigned only to produce a T1-weighted image of nanohybrid samples, the results of which are shown in Fig. 9.

The pictures identify the contrast increase by increasing sample concentration, confirming that positive contrast enhancement depends on the sample concentration analyzed by magnetic nanoparticles [53]. However, at the highest concentration, the contrast in the $CDs@MnFe_2O_4$ and $CDs@CuFe_2O_4$ decreased due to the ethanolamine encapsulation covering the

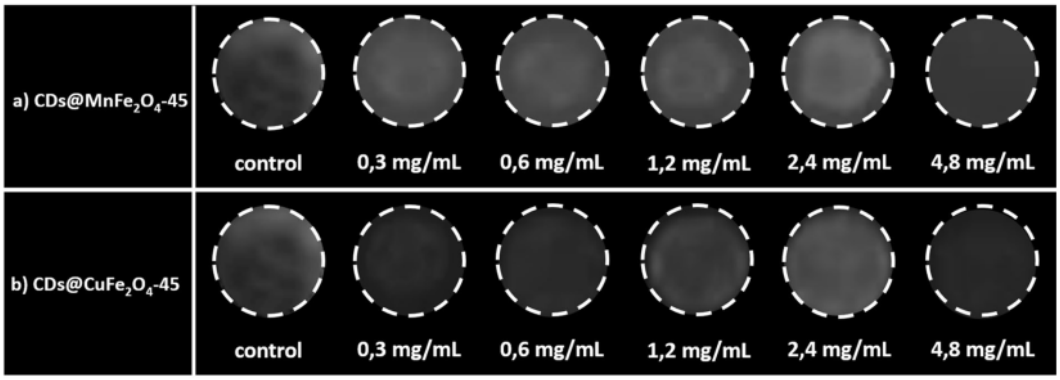

Figure 8: MRI images of (a) $CDs@MnFe_2O_4$ and (b) $CDs@CuFe_2O_4$ on varied nanohybrid concentrations.

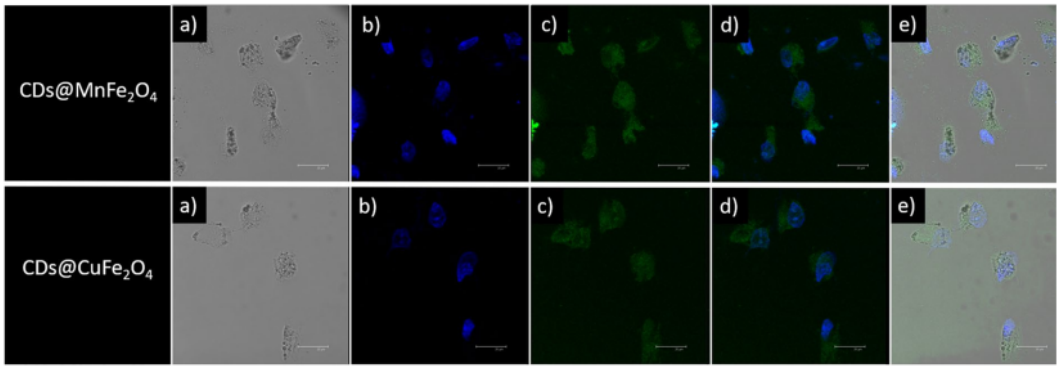

Figure 9: Photograph of CDs@MFe_2O_4 (a) bright field, (b) DAPI marker emission, (c) CDs@MFe_2O_4 emission, (d) Combined DAPI and CDs@MFe_2O_4, and (e) Combined a-d images.

nanohybrids affecting the particle size increased [54]. The particle size is an essential factor in the contrast agent. The more petite particle size performs dipole–dipole interactions between magnetic nanoparticle ions and protons, H_2O will be maximum. This interaction increases longitudinal relativity and causes positive contrast enhancement in T1-weighted images to be brighter in result [47, 55, 56].

Conclusions

$MnFe_2O_4$-ethanolamine and $CuFe_2O_4$-ethanolamine nanohybrids could be synthesized from $Cu(acac)_2$, $Mn(acac)_2$, $Fe(acac)_3$, oleylamine, benzyl ether, and ethanolamine using the solvothermal method. The characterization results showed that $MnFe_2O_4$-ethanolamine and $CuFe_2O_4$-ethanolamine nanohybrids contained CDs from ethanolamine and had magnetic properties from nanoparticles from $MnFe_2O_4$ and $CuFe_2O_4$. The CDs@$MnFe_2O_4$-45 and CDs@$CuFe_2O_4$-45 toxicity tests were performed using the MTT Assay method; the percent viability was higher than 80% with a 250 µg/mL concentration that indicated nanoparticles were non-toxic and the contrast of CDs@$CuFe_2O_4$ gave better images than CDs@$MnFe_2O_4$ at various sample concentrations in MRI analysis. Thus, CDs@MFe_2O_4 potentially applies as a candidate for simultaneous contrast and markers.

Experimental method

Materials

Iron(III) acetylacetonate ($Fe(acac)_3$, 97%, Sigma-Aldrich), manganese(II) acetylacetonate [$Mn(acac)_2$] copper(II) acetylacetonate [$Cu(acac)_2$] (97%, Sigma-Aldrich), oleylamine (70%, Sigma-Aldrich), benzyl ether (98%), ethanolamine (98%), and ethanol (90%, Merck).

Synthesis of carbon nanodots-metal ferrite nanohybrid (CDs@MFe_2O_4)

The synthesis of CDs-MFe_2O_4 nanohybrid was accomplished through one-pot solvothermal method. Briefly, the total amount of (0.70 g $Fe(acac)_3$ and 0.25 g $Mn(acac)_2$) and (0.70 g $Fe(acac)_3$ and 0.26 g $Cu(acac)_2$) were obtained in two parts of a two-neck round bottom flask. While mixing with a magnetic stirrer, 15 mL of oleylamine and 15 mL of benzyl ether were added to the flask. In this method, a 220 V electric pressure thermocouple was used. The first temperature was set at 100 °C for 20 min, then raised at 270 °C for 1 h, and lowered to 150 °C. The formulation (0, 15, 30, and 45 mL) of ethanolamine was injected at 150 °C with heating for an hour (Table 1). The temperature was lowered to 60 °C, and the synthesis process was interrupted. The obtained CDs-MFe_2O_4 were washed with ethanol and centrifugated to accumulate the precipitate. During the solvothermal process, ethanolamine formed CDs by self-assembling, as shown in Scheme 1.

Cell culturing

Culturing the HeLa cell was prepared in Eagle's minimum essential medium (containing 1.5 g L^{-1} sodium bicarbonate) supplemented with 1% L-glutamine, 1% formulation of antibiotic antimycotic, and 10% fetal bovine serum. The cells were cultured in a humified 5% CO_2 incubator maintained at 60 °C for inducing cell expansion and senescence. Before CDs-MFe_2O_4 feeding, HeLa cells were planted in a six-well plate in 2 mL of culturing medium. After 24 h, the HeLa cells were incubated an hour with 300 µL of CDs-MFe_2O_4, rinsed with PBS three times, and fixed for 10 min with 75% alcohol. The resulting cells were incubated for 20 min with 2 mL DAPI in PBS at room temperature to stain the nucleus. HeLa cells

TABLE 1: Formulation CDs@MFe_2O_4-ethanolamine.

No	Nanohybrid		Ethanolamine Composition (mL)
	$MnFe_2O_4$	$CuFe_2O_4$	
1	CDs@$MnFe_2O_4$	CDs@$CuFe_2O_4$	0
2	CDs@$MnFe_2O_4$-15	CDs@$CuFe_2O_4$-15	15
3	CDs@$MnFe_2O_4$-30	CDs@$CuFe_2O_4$-30	30
4	CDs@$MnFe_2O_4$-45	CDs@$CuFe_2O_4$-45	45

were visualized using fluorescence using an inverted Confocal Microscope (Leica Microsystems).

Cytotoxicity assessment

The MTT assay was used to quantify cell viability of HeLa. Culturing HeLa cells was prepared in Eagle's minimum essential medium (25,000 cells per well) for 24 h. After rinsing with phosphate-buffered saline (PBS, Uni Region Biotech, Taiwan), the grown cells were incubated with the set samples for 24 h. The plate was rinsed with PBS twice, added with MTT reagent (1 mL, 500 mg m L^{-1}), and incubated for 4 h. Dimethyl sulfoxide (1 mL) was added to dissolve the formazan crystals in each well and the absorbance was measured using an Elisa reader (Biotech Powerwave XS) at 570 nm. The strength of absorption depends on the number of living cells with different formazan.

Other characterizations

Several techniques characterized the yields. Ultraviolet–Visible (UV–Vis) spectra were recorded using a UV–Vis Shimadzu 1800 spectrophotometer (Shimadzu, Japan). Fourier Transform Infra-Red (FTIR) spectra were recorded using an Infrared (IR) Tracer-100 (Shimadzu, Japan). The photoluminescence of CDs@MFe_2O_4 was collected using an LS 55 Fluorescence Spectrometer (Shimadzu, Japan). Dynamic Light Scattering (DLS) analyses were recorded using Analyser Malvern. X-Ray Diffraction (XRD) diffractograms were recorded using an XRD Philips. Vibrating Sample Magnetometry (VSM) curves were recorded using Lake Shore Cryotronic.

Acknowledgments

The authors thank to Universitas Airlangga for SATU joint research scheme (under Contract 1312/UN3.15/PT/2021), and Indonesian Scholar Education Program of Ministry of Education, Culture and Higher Education-LPDP.

Data availability

We declare that all data generated or analyzed during this study are included in this published article; and the data are available from the corresponding author on reasonable request.

Declarations

Conflict of interest Authors declare that there are no conflicts of interest on present study.

References

1. M.J.F. Calvete, S.M.A. Pinto, M.M. Pereira, C.F.G.C. Geraldes, Metal coordinated pyrrole-based macrocycles as contrast agents for magnetic resonance imaging technologies: synthesis and applications. Coord. Chem. Rev. **333**, 82 (2017)
2. C. Felton, A. Karmakar, Y. Gartia, P. Ramidi, A.S. Biris, A. Ghosh, Magnetic nanoparticles as contrast agents in biomedical imaging: recent advances in iron-and manganese-based magnetic nanoparticles. Drug Metab. Rev. **46**(2), 142 (2014)
3. G.-L. Davies, I. Kramberger, J.J. Davis, Environmentally responsive MRI contrast agents. Chem. Commun. **49**(84), 9704 (2013)
4. F. Du, L. Zhang, L. Zhang, M. Zhang, A. Gong, Y. Tan, J. Miao, Y. Gong, M. Sun, H. Ju, Engineered gadolinium-doped carbon dots for magnetic resonance imaging-guided radiotherapy of tumors. Biomaterials **121**, 109 (2017)
5. J. Li, C. Wu, P. Hou, M. Zhang, K. Xu, One-pot preparation of hydrophilic manganese oxide nanoparticles as T1 nano-contrast agent for molecular magnetic resonance imaging of renal carcinoma in vitro and in vivo. Biosens. Bioelectron. **102**, 1 (2018)
6. V.M. Runge, T. Ai, D. Hao, X. Hu, The developmental history of the gadolinium chelates as intravenous contrast media for magnetic resonance. Investig. Radiol. **46**(12), 807 (2011)
7. H.B. Na, I.C. Song, T. Hyeon, Inorganic nanoparticles for MRI contrast agents. Adv. Mater. **21**(21), 2133 (2009)
8. Y.-K. Peng, S.C.E. Tsang, P.-T. Chou, Chemical design of nanoprobes for T1-weighted magnetic resonance imaging. Mater. Today **19**(6), 336 (2016)
9. B.H. McDonagh, G. Singh, S. Hak, S. Bandyopadhyay, I.L. Augestad, D. Peddis, I. Sandvig, A. Sandvig, W.R. Glomm, L-DOPA-coated manganese oxide nanoparticles as dual MRI contrast agents and drug-delivery vehicles. Small **12**(3), 301 (2016)
10. P.T. Normann, P. Joffe, I. Martinsen, H.S. Thomsen, Quantification of gadodiamide as Gd in serum, peritoneal dialysate and faeces by inductively coupled plasma atomic emission spectroscopy and comparative analysis by high-performance liquid chromatography. J. Pharm. Biomed. Anal. **22**(6), 939 (2000)
11. D. Kim, K.S. Hong, J. Song, The present status of cell tracking methods in animal models using magnetic resonance imaging

technology. Mol. Cells (Springer Science & Business Media BV) **23**(2), 132–7 (2007)

12. A. Barge, G. Cravotto, E. Gianolio, F. Fedeli, How to determine free Gd and free ligand in solution of Gd chelates. A technical note. Contrast Media Mol. Imaging **1**(5), 184 (2006)
13. J. Bennet, R. Tholkappiyan, K. Vishista, N.V. Jaya, F. Hamed, Attestation in self-propagating combustion approach of spinel AFe_2O_4 (A = Co, Mg and Mn) complexes bearing mixed oxidation states: magnetostructural properties. Appl. Surf. Sci. **383**, 113 (2016)
14. Y. Gao, Carbon nano-allotrope/magnetic nanoparticle hybrid nanomaterials as T2 contrast agents for magnetic resonance imaging applications. J. Funct. Biomater. **9**(1), 16 (2018)
15. J. Cai, P. Yi, Y. Miao, J. Liu, Y. Hu, Q. Liu, Y. Feng, H. Chen, L. Li, Ultrasmall T1–T2 magnetic resonance multimodal imaging nanoprobes for the detection of β-amyloid aggregates in Alzheimer's disease mice. ACS Appl. Mater. Interfaces **12**(24), 26812 (2020)
16. L. Del Bianco, F. Spizzo, P. Sgarbossa, E. Sieni, G. Barucca, M.R. Ruggiero, S. GeninattiCrich, Dipolar magnetic interactions in Mn-doped magnetite nanoparticles loaded into PLGA nanocapsules for nanomedicine applications. J. Phys. Chem. C **123**(49), 30007 (2019)
17. Y. Fu, X. Li, H. Chen, Z. Wang, W. Yang, H. Zhang, CXC chemokine receptor 4 antagonist functionalized renal clearable manganese-doped iron oxide nanoparticles for active-tumor-targeting magnetic resonance imaging-guided bio-photothermal therapy. ACS Appl. Bio Mater. **2**(8), 3613 (2019)
18. S. Kanagesan, M. Hashim, S. AbAziz, I. Ismail, S. Tamilselvan, N.B. Alitheen, M.K. Swamy, B. Purna Chandra Rao, Evaluation of antioxidant and cytotoxicity activities of copper ferrite ($CuFe_2O_4$) and zinc ferrite ($ZnFe_2O_4$) nanoparticles synthesized by sol–gel self-combustion method. Appl. Sci. **6**(9), 184 (2016)
19. M. Arruebo, R. Fernández-Pacheco, M.R. Ibarra, J. Santamaría, Magnetic nanoparticles for drug delivery. Nano Today **2**(3), 22 (2007)
20. M. Zhang, W. Wang, N. Zhou, P. Yuan, Y. Su, M. Shao, C. Chi, F. Pan, Near-infrared light triggered photo-therapy, in combination with chemotherapy using magnetofluorescent carbon quantum dots for effective cancer treating. Carbon **118**, 752 (2017)
21. Z. Zhao, J. Bao, C. Fu, M. Lei, J. Cheng, Controllable synthesis of manganese oxide nanostructures from 0-D to 3-D and mechanistic investigation of internal relation between structure and T 1 relaxivity. Chem. Mater. **29**(24), 10455 (2017)
22. Z. Shen, T. Chen, X. Ma, W. Ren, Z. Zhou, G. Zhu, A. Zhang, Y. Liu, J. Song, Z. Li, H. Ruan, W. Fan, L. Lin, J. Munasinghe, X. Chen, A. Wu, Multifunctional theranostic nanoparticles based on exceedingly small magnetic iron oxide nanoparticles for T1-weighted magnetic resonance imaging and chemotherapy. ACS Nano **11**(11), 10992 (2017)
23. I.C. Covaliu, J. Neamtu, G. Georgescu, T. Malaeru, C. Cristea, I. Jitaru, Synthesis and characterization of ferrites (Fe_3O_4/$CuFe_2O_4$)-calcium alginate hybrids for magnetic resonance imaging. Dig. J. Nanomater. Biostruct. **6**(1), 245 (2011)
24. P. Zuo, X. Lu, Z. Sun, Y. Guo, H. He, A review on syntheses, properties, characterization and bioanalytical applications of fluorescent carbon dots. Microchim Acta **183**(2), 519 (2016)
25. X. Xu, R. Ray, Y. Gu, H.J. Ploehn, L. Gearheart, K. Raker, W.A. Scrivens, Electrophoretic analysis and purification of fluorescent single-walled carbon nanotube fragments. J. Am. Chem. Soc. **126**(40), 12736 (2004)
26. X. Sun, Y. Lei, Fluorescent carbon dots and their sensing applications. TRAC Trends Anal. Chem. **89**, 163 (2017)
27. Y. Liu, L. Feng, T. Liu, L. Zhang, Y. Yao, D. Yu, L. Wang, N. Zhang, Multifunctional pH-sensitive polymeric nanoparticles for theranostics evaluated experimentally in cancer. Nanoscale **6**(6), 3231 (2014)
28. L. Cao, X. Wang, M.J. Meziani, F. Lu, H. Wang, P.G. Luo, Y. Lin, B.A. Harruff, L.M. Veca, D. Murray, Carbon dots for multiphoton bioimaging. J. Am. Chem. Soc. **129**(37), 11318 (2007)
29. B. Wang, H. Tan, T. Zhang, W. Duan, Y. Zhu, Hydrothermal synthesis of N-doped carbon dots from an ethanolamine–ionic liquid gel to construct label-free multifunctional fluorescent probes for Hg^{2+}, Cu^{2+} and $S_2O_3^{2-}$. Analyst **144**(9), 3013 (2019)
30. C. Zhang, H. Zhang, Y. Yu, S. Wu, F. Chen, Ratio fluorometric determination of ATP base on the reversion of fluorescence of calcein quenched by Eu(III) ion using carbon dots as reference. Talanta **197**, 451 (2019)
31. X. Dong, Y. Su, H. Geng, Z. Li, C. Yang, X. Li, Y. Zhang, Fast one-step synthesis of N-doped carbon dots by pyrolyzing ethanolamine. J. Mater. Chem. C **2**(36), 7477 (2014)
32. I.Y. Goryacheva, A.V. Sapelkin, G.B. Sukhorukov, Carbon nanodots: mechanisms of photoluminescence and principles of application. TRAC Trends Anal. Chem. **90**, 27 (2017)
33. J. Shen, Y. Zhu, X. Yang, C. Li, Graphene quantum dots: emergent nanolights for bioimaging, sensors, catalysis and photovoltaic devices. Chem. Commun. **48**(31), 3686 (2012)
34. Y.-F. Kang, Y.-W. Fang, Y.-H. Li, W. Li, X.-B. Yin, Nucleus-staining with biomolecule-mimicking nitrogen-doped carbon dots prepared by a fast neutralization heat strategy. Chem. Commun. **51**(95), 16956 (2015)
35. Y. Chen, H. Lian, Y. Wei, X. He, Y. Chen, B. Wang, Q. Zeng, J. Lin, Concentration-induced multi-colored emissions in carbon dots: origination from triple fluorescent centers. Nanoscale **10**(14), 6734 (2018)
36. H. Nagai, Y.H. Kim, Cancer prevention from the perspective of global cancer burden patterns. J. Thorac. Dis. **9**(3), 448 (2017)
37. M.Z. Fahmi, J.-Y. Chang, A facile strategy to enable nanoparticles for simultaneous phase transfer, folate receptor targeting, and cisplatin delivery. RSC Adv. **4**(100), 56713 (2014)

38. J. Dulińska-Litewka, A. Łazarczyk, P. Hałubiec, O. Szafrański, K. Karnas, A. Karewicz, Superparamagnetic iron oxide nanoparticles—current and prospective medical applications. Materials **12**(4), 617 (2019)
39. H. Li, X. He, Y. Liu, H. Huang, S. Lian, S.-T. Lee, Z. Kang, One-step ultrasonic synthesis of water-soluble carbon nanoparticles with excellent photoluminescent properties. Carbon **49**(2), 605 (2011)
40. A. Wibrianto, S.Q. Khairunisa, S.C.W. Sakti, Y.L. Ni'mah, B. Purwanto, M.Z. Fahmi, Comparison of the effects of synthesis methods of B, N, S, and P-doped carbon dots with high photoluminescence properties on HeLa tumor cells. RSC Adv. **11**(2), 1098 (2021)
41. S. Kumar, R.R. Nair, P.B. Pillai, S.N. Gupta, M.A.R. Iyengar, A.K. Sood, Graphene oxide–$MnFe_2O_4$ magnetic nanohybrids for efficient removal of lead and arsenic from water. ACS Appl. Mater. Interfaces **6**(20), 17426 (2014)
42. I.O.P. De Berti, M.V. Cagnoli, G. Pecchi, J.L. Alessandrini, S.J. Stewart, J.F. Bengoa, S.G. Marchetti, Alternative low-cost approach to the synthesis of magnetic iron oxide nanoparticles by thermal decomposition of organic precursors. Nanotechnology. **24**(17), 175601 (2013)
43. Y. Wang, A. Hu, Carbon quantum dots: synthesis, properties and applications. J. Mater. Chem. C **2**(34), 6921 (2014)
44. A. Rampino, M. Borgogna, P. Blasi, B. Bellich, A. Cesàro, Chitosan nanoparticles: preparation, size evolution and stability. Int. J. Pharm. **455**(1–2), 219 (2013)
45. D.J. McClements, *Food Emulsions: Principles, Practices, and Techniques* (CRC Press, Boca Raton, 2004)
46. A.K. Zak, W.H.A. Majid, M.E. Abrishami, R. Yousefi, X-ray analysis of ZnO nanoparticles by Williamson–Hall and size–strain plot methods. Solid State Sci. **13**(1), 251 (2011)
47. M.Z. Fahmi, D.L.N. Wibowo, S.C.W. Sakti, H.V. Lee, Human serum albumin capsulated hydrophobic carbon nanodots as staining agent on HeLa tumor cell. Mater. Chem. Phys. **239**, 122266 (2020)
48. D.J. Craik, *Structure and Properties of Magnetic Materials* (Pion, London, 1971)
49. J.C. Stockert, A. Blázquez-Castro, M. Cañete, R.W. Horobin, Á. Villanueva, MTT assay for cell viability: intracellular localization of the formazan product is in lipid droplets. Acta Histochem. **114**(8), 785 (2012)
50. M.Z. Fahmi, A. Haris, A.J. Permana, D.L.N. Wibowo, B. Purwanto, Y.L. Nikmah, A. Idris, Bamboo leaf-based carbon dots for efficient tumor imaging and therapy. RSC Adv. **8**(67), 38376 (2018)
51. A. Permadi, M.Z. Fahmi, J.-K. Chen, J.-Y. Chang, C.-Y. Cheng, G.-Q. Wang, K.-L. Ou, Preparation of poly (ethylene glycol) methacrylate coated $CuInS_2$/ZnS quantum dots and their use in cell staining. RSC Adv. **2**(14), 6018 (2012)
52. A. Kumar, B. Sahoo, A. Montpetit, S. Behera, R.F. Lockey, S.S. Mohapatra, Development of hyaluronic acid–Fe_2O_3 hybrid magnetic nanoparticles for targeted delivery of peptides. Nanomed.: Nanotechnol. Biol. Med. **3**(2), 132 (2007)
53. Y. Pan, J. Yang, Y. Fang, J. Zheng, R. Song, C. Yi, One-pot synthesis of gadolinium-doped carbon quantum dots for high-performance multimodal bioimaging. J. Mater. Chem. B **5**(1), 92 (2017)
54. M.Z. Fahmi, J.-K. Chen, C.-C. Huang, Y.-C. Ling, J.-Y. Chang, Phenylboronic acid-modified magnetic nanoparticles as a platform for carbon dot conjugation and doxorubicin delivery. J. Mater. Chem. B **3**(27), 5532 (2015)
55. C. Yu, T. Xuan, Y. Chen, Z. Zhao, X. Liu, G. Lian, H. Li, Gadolinium-doped carbon dots with high quantum yield as an effective fluorescence and magnetic resonance bimodal imaging probe. J. Alloys Compd. **688**, 611 (2016)
56. C. Zheng, X. An, J. Gong, Novel pH sensitive N-doped carbon dots with both long fluorescence lifetime and high quantum yield. RSC Adv. **5**(41), 32319 (2015)

C11 In situ tailoring of carbon dots-metal ferrite nanohybrid as multipurpose marker agent of HeLa cancer cells

ORIGINALITY REPORT

14%	7%	11%	1%
SIMILARITY INDEX	INTERNET SOURCES	PUBLICATIONS	STUDENT PAPERS

PRIMARY SOURCES

1	S. Radin, P. Ducheyne, B. Rothman, A. Conti. "The effect ofin vitro modeling conditions on the surface reactions of bioactive glass", Journal of Biomedical Materials Research, 1997 Publication	1%
2	Yanyan Liu, Xiaochun Ye, Bingwei Zhou, Zhitao Tian, Caiying Liu, Kaiyuan Li. "Potentially toxic elements in smoke particles and residual ashes by biomass combustion from Huangshi National Mine Park, China", Environmental Geochemistry and Health, 2022 Publication	1%
3	Sameh Ahmed Refaat, Walid Mohammed Abdelmageed, Hadil Magdy Alwedeny, Mohammed Abdelmoneim Fouly, Ehab Hussein Soliman. "Ultrasound Guided Erector Spinae Block Using Bupivacaine - Magnesium Sulphate Versus Bupivacaine - Dexmedetomidine in Lumbar Spine Surgeries.	1%

A Prospective Randomized Trial", Research Square Platform LLC, 2023
Publication

4	www.jove.com Internet Source	<1%
5	Bryan Ronain Smith, Sanjiv Sam Gambhir. "Nanomaterials for In Vivo Imaging", Chemical Reviews, 2017 Publication	<1%
6	Jingjing Li, Chen Wu, Pingfu Hou, Min Zhang, Kai Xu. "One-pot preparation of hydrophilic manganese oxide nanoparticles as T 1 nano-contrast agent for molecular magnetic resonance imaging of renal carcinoma in vitro and in vivo", Biosensors and Bioelectronics, 2018 Publication	<1%
7	d-nb.info Internet Source	<1%
8	researchoutput.ncku.edu.tw Internet Source	<1%
9	Baogang Wang, Hui Tan, Tailiang Zhang, Wenmeng Duan, Yuanqiang Zhu. " Hydrothermal synthesis of N-doped carbon dots from an ethanolamine–ionic liquid gel to construct label-free multifunctional	<1%

fluorescent probes for Hg , Cu and S O ", The Analyst, 2019
Publication

10	Submitted to National Chung Hsing University Student Paper	<1 %
11	Sujin Cho, On Hwang, Iljea Lee, Gayoung Lee, Donghyuck Yoo, Gilson Khang, Peter M. Kang, Dongwon Lee. "Chemiluminescent and Antioxidant Micelles as Theranostic Agents for Hydrogen Peroxide Associated-Inflammatory Diseases", Advanced Functional Materials, 2012 Publication	<1 %
12	Submitted to National University of Singapore Student Paper	<1 %
13	Submitted to Swinburne University of Technology Student Paper	<1 %
14	Lam, F.L.Y.. "A high performance bimetallic catalyst for photo-Fenton oxidation of Orange II over a wide pH range", Catalysis Communications, 200712 Publication	<1 %
15	Lavanya Thyda, Gnyaneshwar Dasi, M.S. Abdul Azeez, K. Naresh et al. "Solution processed highly transparent nitrogen-doped carbon quantum dots/ZnO hybrid thin films: A	<1 %

study on structural and enhanced UV emission", Applied Surface Science, 2023
Publication

16	downloads.hindawi.com Internet Source	<1 %
17	nanoscalereslett.springeropen.com Internet Source	<1 %
18	Hyon Bin Na. "Inorganic Nanoparticles for MRI Contrast Agents", Advanced Materials, 03/03/2009 Publication	<1 %
19	Xiang Wang, Chunlin Li, Hansong Jin, Xingyan Wang et al. "Mutual Promotion of Oxidative Stress Amplification and Calcium Overload by Degradable Spatially Selective Self-Cascade Catalyst for Synergistic Tumor Therapy", Chemical Engineering Journal, 2022 Publication	<1 %
20	dl.uctm.edu Internet Source	<1 %
21	www.webmedcentral.com Internet Source	<1 %
22	Huan Zhang, Li Li, Xiao Li Liu, Ju Jiao et al. " Ultrasmall Ferrite Nanoparticles Synthesized Dynamic Simultaneous Thermal Decomposition for High-Performance and	<1 %

Multifunctional Magnetic Resonance Imaging Contrast Agent ", ACS Nano, 2017
Publication

23	Rui Hao. "Synthesis, Functionalization, and Biomedical Applications of Multifunctional Magnetic Nanoparticles", Advanced Materials, 05/14/2010 Publication	<1 %
24	pugno.dicam.unitn.it Internet Source	<1 %
25	www.rsc.org Internet Source	<1 %
26	Gong, Xiaojuan, Wenjing Lu, Man Chin Paau, Qin Hu, Xin Wu, Shaomin Shuang, Chuan Dong, and Martin M.F. Choi. "Facile synthesis of nitrogen-doped carbon dots for Fe3+ sensing and cellular imaging", Analytica Chimica Acta, 2015. Publication	<1 %
27	Ruichan Lv, Piaoping Yang, Fei He, Shili Gai, Chunxia Li, Yunlu Dai, Guixin Yang, Jun Lin. "A Yolk-like Multifunctional Platform for Multimodal Imaging and Synergistic Therapy Triggered by a Single Near-Infrared Light", ACS Nano, 2015 Publication	<1 %
28	bmcchem.biomedcentral.com Internet Source	

		<1%
29	clok.uclan.ac.uk Internet Source	<1%
30	ebin.pub Internet Source	<1%
31	www.nature.com Internet Source	<1%
32	www.thieme-connect.com Internet Source	<1%
33	"Magnetic Nanoheterostructures", Springer Science and Business Media LLC, 2020 Publication	<1%
34	Fahmi, Mochamad Zakki, Jem-Kun Chen, Chih-Ching Huang, Yong-Chien Ling, and Jia-Yaw Chang. "Phenylboronic acid-modified magnetic nanoparticles as a platform for carbon dot conjugation and doxorubicin delivery", Journal of Materials Chemistry B, 2015. Publication	<1%
35	Flavio Bonati, Giovanni Minghetti. "Mercury(II) derivatives of acetylacetone", Journal of Organometallic Chemistry, 1970 Publication	<1%

36	Guoyong Liu, Jiahui Zhao, Shuang Wang, Shasha Lu, Jian Sun, Xiurong Yang. "Enzyme-induced in situ generation of polymer carbon dots for fluorescence immunoassay", Sensors and Actuators B: Chemical, 2020 Publication	<1 %
37	Lertsutthiwong, P.. "Preparation of alginate nanocapsules containing turmeric oil", Carbohydrate Polymers, 20081016 Publication	<1 %
38	Liheng Wu, Adriana Mendoza-Garcia, Qing Li, Shouheng Sun. "Organic Phase Syntheses of Magnetic Nanoparticles and Their Applications", Chemical Reviews, 2016 Publication	<1 %
39	Ozioma Udochukwu Akakuru, M. Zubair Iqbal, Madiha Saeed, Chuang Liu et al. " The Transition from Metal-Based to Metal-Free Contrast Agents for Magnetic Resonance Imaging Enhancement ", Bioconjugate Chemistry, 2019 Publication	<1 %
40	S. Sabalanvand, H. Hazrati, Y. Jafarzadeh, A. Jafarizad, S. Gharibian. "Investigation of Ag and magnetite nanoparticle effect on the membrane fouling in membrane bioreactor", International Journal of Environmental Science and Technology, 2021	<1 %

	Publication	
41	Yinping Zhuang, Shaohui Zheng, Qi Liu, Kai Xu, Cuiping Han, Deqiang Cheng. " Preparation of Carbon Dots for Effective Fluorescence Imaging of Ovarian Cancer Cells and Brain Imaging ", Nano, 2020 Publication	<1 %
42	aei.pitt.edu Internet Source	<1 %
43	coek.info Internet Source	<1 %
44	discovery.ucl.ac.uk Internet Source	<1 %
45	epub.uni-regensburg.de Internet Source	<1 %
46	kth.diva-portal.org Internet Source	<1 %
47	ojs.nassg.org Internet Source	<1 %
48	spj.science.org Internet Source	<1 %
49	tel.archives-ouvertes.fr Internet Source	<1 %
50	www.hindawi.com Internet Source	<1 %

51 Claudia Coughlan, Maria Ibáñez, Oleksandr Dobrozhan, Ajay Singh, Andreu Cabot, Kevin M. Ryan. "Compound Copper Chalcogenide Nanocrystals", Chemical Reviews, 2017
Publication

<1%

Exclude quotes	On	Exclude matches	< 5 words
Exclude bibliography	On		